Optics Letters

Polarized imaging interpreter for simultaneous clocking metrology of multiple objects

Hyo Bin Jeong,[1] Jong-Kyu Park,[1] Daewook Kim,[2] and Ki-Nam Joo[1,*]

[1]Department of Photonic Engineering, Chosun University, 309 Pilmun-daero, Dong-gu, Gwangju 61452, Republic of Korea
[2]Wyant College of Optical Sciences, University of Arizona, 1630 E. University Blvd., Tucson, Arizona 85721, USA
*Corresponding authors: knjoo@chosun.ac.kr

Received 3 August 2021; revised 6 September 2021; accepted 10 September 2021; posted 13 September 2021 (Doc. ID 439614); published 30 September 2021

A polarized imaging interpreter to simultaneously measure rotational angles of multiple objects is proposed and experimentally verified. Based on the multiplexed optical configuration using a polarization pixelated camera, the proposed sensor has the unique feature to precisely monitor the standard and the non-standard clocking motions in static or dynamic applications at once.

https://doi.org/10.1364/OL.439614

A rotational (i.e., clocking) motion of an object needs to be measured for various dynamic applications such as rotary actuators [1], segmented active optics, spindles [2], and rotating plates [3]. In the meantime, the rotational motion metrology is also very important to find out the rotational positions of the static objects such as mechanically assembled components [4], robotics [5], and segmented mirrors [6]. Also, for the extremely large next-generation space telescope missions, aperture segmentation (e.g., hexagonal primary mirrors) or scalable telescope architecture becomes essential [7]. The segmented optics are often designed in a way that they create a single coherent optical surface as if they were a monolithic optical surface. Especially, off-axis segments (e.g., off-axis parabolic mirror) must maintain their rigid-body alignment (e.g., 6 or 5 deg of freedom) such as relative position in their array, clocking, tip-tilt, and/or co-phasing among them [7,8].

Optical sensors are very attractive to be applied for dynamic and static applications because they can precisely measure the motion with high speed through non-contact approaches. Moreover, they are not sensitive to electromagnetic noise due to the unit under test itself. Most common optical sensors to measure rotational motions are optical rotary encoders [9,10], which have moving disks with concentric tracks. However, one of the drawbacks of the optical encoder is that the number of sensors and its controllers should increase as multiple measurement objects are added. It is important to note that most traditional approaches are not scalable, so they have limitations for large-scale simultaneous applications.

The polarization of light is a very useful feature to recognize, measure, and analyze the light signal in an optical system. By Malus's law, the irradiance variation is a function of the rotation angle of the polarizer, widely used in various fields such as photoelasticity [11,12] and light attenuation [13], and it has been used as a rotational motion sensor [14,15]. Furthermore, Stokes polarimetry has been proposed to measure polarization properties of a material with linear, circular polarization states of light, and it was used for a roll angle sensor at a specific point [16,17].

In this Letter, we propose a scalable and instantaneous (so, it can be simultaneous for multiple objects without a temporal scanning process) imaging sensor to monitor the rotational motions of several objects at once. As far as we know, this imaging rotational clocking sensor is first proposed and verified. This imaging sensor can interpret the polarized images by a polarization pixelated CMOS camera (PPCMOS) and determine the clocking angles. Figure 1 shows the schematics of a polarized imaging interpreter (PI^2) proposed in this investigation. A randomly polarized light from a fiber-coupled LED is reflected off by a beam splitter (BS) after passing through a collimating lens (CL). The reflected light goes toward a linear polarizer (P) attached to a rotating object and reflected off by the P. The polarization status of the light is orthogonal to the transmission axis of the P, and the light is captured by a PCMOS. In a PCMOS, four polarizers with the transmission axes of 0°, 45°, 90°, and 135°, respectively, as an array format, are spatially multiplexed in front of an imaging sensor [18] as shown in the inset of Fig. 1. The whole images obtained by the PCMOS are divided into four images, following Malus's law, and they are mathematically described as

$$\begin{aligned} I_0 &= I_i \cos^2(\varphi) = (I_i/2)\,[1+\cos(2\varphi)]\,, \\ I_{45} &= I_i \cos^2(45^\circ-\varphi) = (I_i/2)\,[1+\sin(2\varphi)]\,, \\ I_{90} &= I_i \cos^2(90^\circ-\varphi) = (I_i/2)\,[1-\cos(2\varphi)]\,, \\ I_{135} &= I_i \cos^2(45^\circ+\varphi) = \left(\frac{I_i}{2}\right)[1-\sin(2\varphi)]\,, \end{aligned} \tag{1}$$

where I_i and φ are the irradiance and the polarization angle of the light incident to the PCMOS, respectively. The polarization angle φ can be adjusted by the rotation of the P. I_0, I_{45}, I_{90}, and I_{135} are the irradiances of the light transmitted through four kinds of polarizers. It is noted that the lateral coordinate of imaging plane is ignored for simplicity. From Eq. (1), φ can be

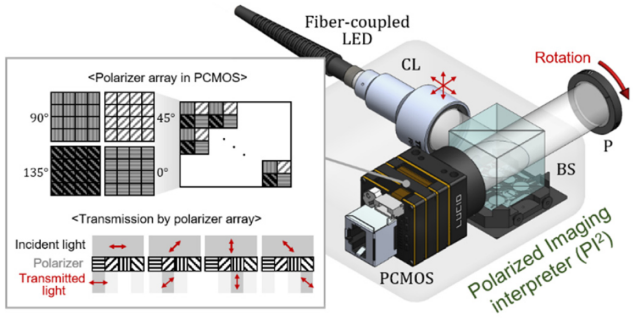

Fig. 1. Schematic of a polarized imaging interpreter (PI^2); CL, collimating lens; BS, beam splitter; P, linear polarizer; PCMOS, polarization pixelated CMOS camera. The inset describes an inner polarizer array of the PCMOS and its transmission functionality.

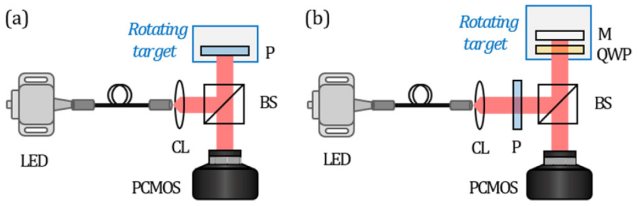

Fig. 2. Optical configurations of (a) basic PI^2 and (b) resolution-enhanced PI^2; CL, collimating lens; BS, beam splitter; P, linear polarizer; QWP, quarter-wave plate; M, mirror; PCMOS, polarization pixelated CMOS camera.

calculated as

$$\varphi = \tan^{-1}\left[\frac{I_{45} - I_{135}}{I_0 - I_{90}}\right]/2. \quad (2)$$

It is critical to note that PI^2 can directly provide the polarization angle of the P by using Eq. (2) and is not affected by the optical power fluctuations of the optical source.

Moreover, PI^2 can enhance the measurement resolution of the rotation angle with the aid of adopting a quarter-wave plate (QWP). Compared to the basic concept of PI^2 as shown in Fig. 2(a), the initial light is linearly polarized and passes through a QWP twice before the acquisition of the image as shown in Fig. 2(b), which is equivalent to going through a half-wave plate as a linear polarization rotator. When the QWP and a mirror (M) are attached to the rotating target, the rotation angle (φ') can be determined by

$$\varphi' = \tan^{-1}\left[\frac{I_{45} - I_{135}}{I_0 - I_{90}}\right]/4. \quad (3)$$

As known in Eq. (3), the measurement resolution (i.e., sensitivity) becomes twice better than that of the basic configuration.

In order to verify the actual performances, a series of feasibility tests were implemented for basic and resolution-enhanced versions of PI^2. In the basic PI^2, a warm white LED with a 600 nm center wavelength and a 130 nm bandwidth was used as an optical source, and a commercial PCMOS (PHX050S-PC, Lucid) with (2448 × 2048) pixels captured the whole image and divided it into four images. A linear polarizer was attached to stepping motorized rotary stage and rotated for 720° with 1° incremental steps. The light spot on the image was reduced

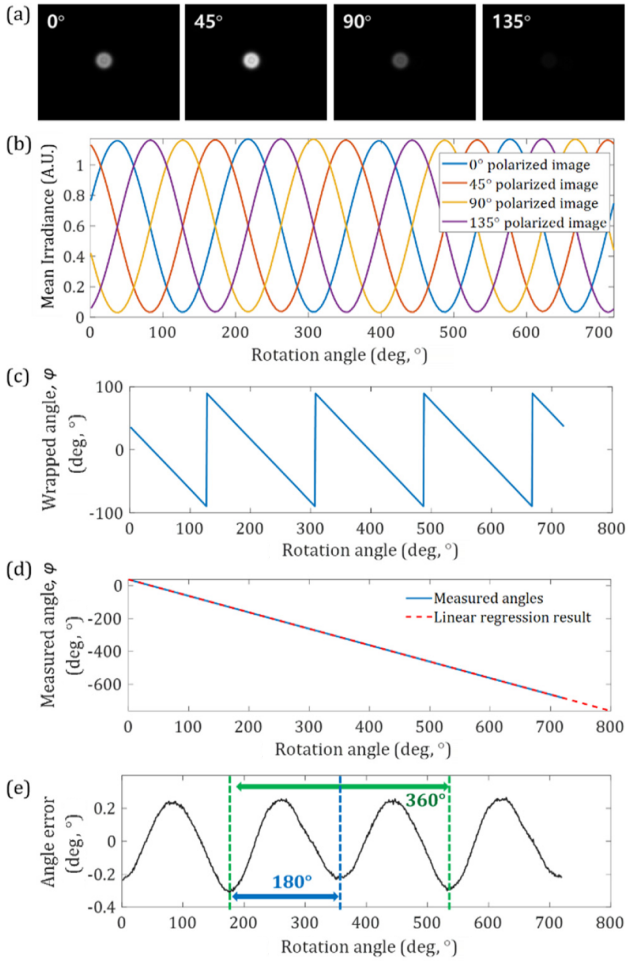

Fig. 3. (a) Light spots of four polarized images, (b) mean irradiance variations of four polarized images along the rotation of the polarizer, (c) wrapped angle (φ), (d) measured rotation angle (φ), and (e) nonlinear angle error by the linear regression of (d).

as ∼1 mm to avoid the measurement errors caused by cutting off the beam spot by the imaging area as shown in Fig. 3(a). The mean irradiance of each light spot of Fig. 3(a) was calculated, and its variations along the rotation of the P were obtained as shown in Fig. 3(b). As shown in Fig. 3(b), the mean irradiance variations of four polarized images are phase-shifted with $\pi/2$ as predicted in Eq. (1), and the rotation angles were calculated as shown in Fig. 3(c) by Eq. (2).

As shown in Fig. 3(c), the wrapped clocking angle had the period of 180°, which means the measurement resolution is twice better than the physical rotation angle of the P as expected in Eq. (2). With the aid of phase-unwrapping, the measured rotation angles well agreed with those of the P as Fig. 3(d), clockwise rotated, as the linear slope of −1.00003, but they have nonlinear errors as shown in Fig. 3(e). These nonlinear errors include two kinds of periodic errors with 180° and 360° periods, and their magnitudes were 0.25° and 0.03°, respectively, as the results of Fourier amplitude. The periodic errors of PI^2 are originated from the unexpected light by ghost reflections, retardations of the uncalibrated BS [17], and the extinction ratios of a target polarizer and four polarizers in the PCMOS. However, these periodic errors are systematic errors, which can be calibrated and compensated with the as-manufactured

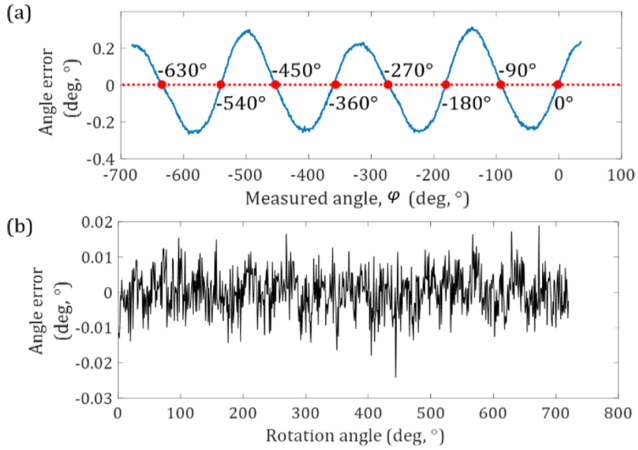

Fig. 4. (a) Periodic error versus measured rotation angle (φ) with zero crossing points at ($m \times 90°$) and (b) nonlinear angle error after the compensation.

system's measurement results. As shown in Fig. 4(a), the periodic error became zero when the measured rotation angles were ($m \times 90°$), where m is an integer. Once the periodic errors were collected from ($\varphi = 0°$) to ($\varphi = \pm 360°$) in a lookup table, the calibrated results could be obtained with the subtraction of the systematic-and-periodic errors. In this investigation, we acquired and modeled the lookup table as periodic errors, fitted with sinusoidal functions for mathematical modeling (Supplement 1). Then, the measurement results were compensated as shown in Fig. 4(b). The residual nonlinear errors were less than $\pm 0.02°$ with the standard deviation of $0.006°$.

The same procedure was repeated for the resolution-enhanced version of PI^2. The final wrapped angle had the period of 90° with the 4 times better resolution as shown in Fig. 5(a), and the measured rotation angle was linear to the real rotation of the stage in Fig. 5(b). The dominant periodic errors have the periodicities of 90°, 180°, and 360° with 041°, 025°, and 0.04° amplitudes, respectively, as the results of Fourier amplitudes. After the compensation of periodic errors, the remaining nonlinear errors were less than $\pm 0.03°$, and their standard deviation was $0.023°$. This remaining error can be self-calibrated by fitting the Stokes parameters [17]. Furthermore, in order to achieve the highest precision and accuracy by reducing the periodic error, a monochromatic light can be used with the wavelength-matching QWP, BS, and P in the system. For most applications, however, PI^2 is designed for the purpose of a robust sensing device with any kind of light sources.

To demonstrate the resolution of the as-built PI^2 and its resolution-enhanced version, the targets were rotated with $0.01°$ of the minimum incremental angle of the stepping motorized stage. As the result, both types of the system were able to sufficiently resolve $0.01°$. In addition, the measurement error caused by the tilt motions of the target was investigated because the polarization properties can be affected by the axis tilt of the polarized elements with respect to the incident beam [19]. The variation of the measurement results was less than $0.02°$ in the range of $\pm 1°$ of the tilt variation (Supplement 1).

A unique feature of PI^2 is that it does not require an illuminating light source in the system, and it can use a natural light to observe rotating targets as shown in Fig. 6(a). In this investigation, a science kit that simulates the "Sun-Earth-Moon" motion

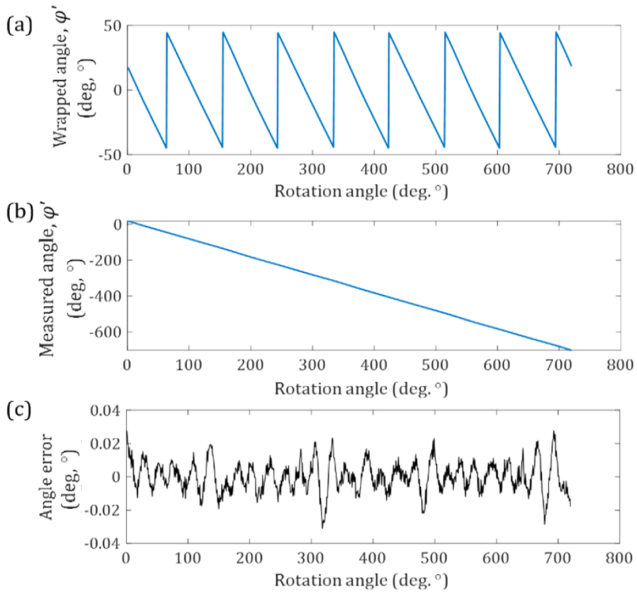

Fig. 5. (a) Wrapped angle (φ'), (b) measured rotation angle (φ'), and (c) nonlinear angle error after the compensation in the resolution enhanced version of PI^2.

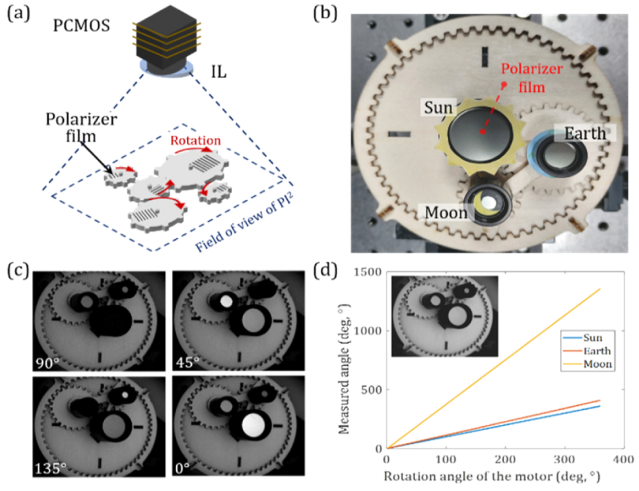

Fig. 6. (a) PI^2 using a natural light to observe multiple targets simultaneously, (b) a scientific kit of "Sun-Earth-Moon" motion simulator, (c) four polarized images captured by the PCMOS (see Visualization 1), and (d) rotational angles of three planets with the original image of (b) (see Visualization 2).

used a demonstration case as shown in Fig. 6(b) to show the capability of simultaneous monitoring the rotational motions of multiple targets without specific light source. The pieces of polarizer film were attached to the "planets," and the "Sun" was rotated with a dc motor. As the motor was operated, three targets were rotated with their own rotating speeds, and the series of instantaneous images was collected. Figure 6(c) shows four polarized images at a specific rotational angle of the motor. As the result, their rotational angles were calculated as shown in Fig. 6(d), well matched to the gear ratios of the kit. In addition, as a benchmark, a typical imaging-based movie of the model kit independent of the polarization of the incident light was obtained by summing of the four polarized images.

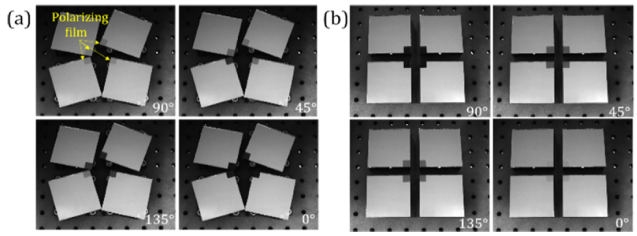

Fig. 7. Four segmented mirrors with (a) the rotational misalignments and (b) the proper alignments.

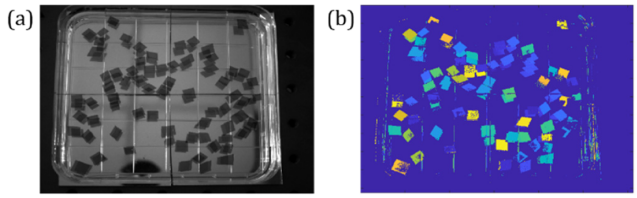

Fig. 8. (a) Image and (b) rotational angle of polarizing film pieces by random water flow (see Visualization 3).

The proposed PI^2 can be also used to confirm the rotational alignment status of several objects such as the segmented and/or active mirrors as shown in Fig. 7. Especially, for off-axis or free-form segments, the segments should be precisely positioned and aligned not only tip and tilt, but also clocking in order to achieve a nominal optical configuration without wavefront aberration due to the rotational shearing. Unfortunately, the rotations of multiple segments (e.g., 10 s to 100 s of next-generation astronomical telescopes) are not easy to be monitored or precisely measured with conventional techniques. However, PI^2 has the capability to monitor the rotation of the segmented mirrors as shown in Fig. 7. A small piece of polarizing film is attached on the edge portion of each segmented mirror, and PI^2 obtained the whole image of all the mirror segments in a single field of view of the multiplexed camera. Based on the irradiances corresponding to the film areas of four polarized images, PI^2 calculated the rotation angles of the mirrors. As the result, the mirrors were relatively rotated, and their relative rotation angles were also calculated as $-11.4°$, $-21.1°$, $17.8°$, and $-12.3°$, respectively. After adjustment of the rotations, the mirrors were able to be properly aligned within $0.1°$ as shown in Fig. 7(b).

Another scientific application field of PI^2 is to monitor the vector flow motions, very important in fluid mechanics and hydrodynamics [20]. Typically, small particles are contained in fluid, and the flow motions can be detected as the positions of the particles by imaging techniques, but the rotational motions of the particles are difficult to be monitored based on traditional imaging approaches. In contrast, PI^2 is beneficial to measuring all of the flow motions such as translational-and-rotational ones. Figure 8 shows the flow motion monitored by PI^2 with small pieces of polarizing films on the water. In the typical image as shown in Fig. 8(a), the rotational motions of the film pieces were not easy to be monitored, but the fluid motion distribution was conveniently monitored by PI^2, where the color indicated the local clocking angles of the particles. With the aid of the stroboscopic technique, PI^2 can be used for measuring high speed rotational motions [21].

In this Letter, we presented and experimentally verified a simultanious imaging rotation sensor, namely, a polarized imaging interpreter (PI^2) using a multiplexed polarization camera. Based on the simple optical configuration using the PCMOS, PI^2 has the unique and scalable feature to monitor the clocking motions of many objects at once as long as they are in a field of view of the system. In order to verify the actual performances of PI^2, the rotation angles were measured using various experimental setups, and the nonlinear errors were estimated to be less than $\pm 0.02°$ with the compensation of the periodic errors. The resolution-enhanced version of PI^2 was also introduced, and a real-time vector field metrology application was introduced to show the benefit of PI^2.

Funding. Chosun University (2021).

Disclosures. The authors declare no conflicts of interest.

Data availability. Data underlying the results presented in this Letter are not publicly available at this time but may be obtained from the authors upon reasonable request.

Supplemental document. See Supplement 1 for supporting content.

REFERENCES

1. X. Sun, W. Chen, J. Zhang, R. Zhou, and W. Chen, Sens. Actuators A **224**, 78 (2015).
2. C. H. Liu, W. Y. Jywe, and H. W. Lee, Meas. Sci. Technol. **15**, 1733 (2004).
3. L. Larsson, M. Sjödahl, and F. Thuvander, Opt. Lasers Eng. **41**, 767 (2004).
4. Y. Jia, S. Li, Y. Qin, and R. Cheng, IEEE Sens. J. **18**, 2023 (2018).
5. K. M. Lee and D. Zhou, IEEE ASME Trans. Mechatron. **9**, 499 (2004).
6. G. Chanan, D. G. MacMartin, J. Nelson, and T. Mast, Appl. Opt. **43**, 1223 (2004).
7. D. Kim, H. Choi, T. Brendel, H. Quach, M. Esparza, H. Kang, Y.-T. Feng, J. N. Ashcraft, X. Ke, T. Wang, and E. S. Douglas, Opto-Electron. Adv. **4**, 210040 (2021).
8. I. Trumper, B. T. Jannuzi, and D. Kim, Opt. Lasers Eng. **104**, 22 (2018).
9. G. Ye, H. Liu, Y. Ban, Y. Shi, L. Yin, and B. Lu, Opt. Commun. **411**, 126 (2018).
10. J. Deng, X. Yan, C. Wei, Y. Lu, M. Li, X. Xiang, W. Jia, and C. Zhou, Appl. Opt. **57**, 2366 (2018).
11. M. S. B. Fernández, Opt. Lasers Eng. **117**, 29 (2019).
12. A. S. Alenin, F. Bashar, M. E. Gehm, and J. S. Tyo, Opt. Lett. **43**, 5789 (2018).
13. J. C. Liang and H. C. Wang, Opt. Lett. **42**, 3654 (2017).
14. D. Y. Guo, L. M. Chang, C. W. Chen, C. C. Li, H. C. Jau, C. T. Wang, W. S. Kuo, and T. H. Lin, Optica **8**, 364 (2021).
15. X. Shan, L. Deng, Q. Dai, Z. Zhou, C. Liang, Z. Li, and G. Zheng, Opt. Express **28**, 26359 (2020).
16. X. Chen, J. Liao, H. Gu, Y. Shi, H. Jiang, and S. Liu, Sens. Actuators A **291**, 144 (2019).
17. X. Chen, J. Liao, H. Gu, C. Zhang, H. Jiang, and S. Liu, Nanomanuf. Metrol. **3**, 228 (2020).
18. Y. B. Seo, H. B. Jeong, H. G. Rhee, Y. S. Ghim, and K.-N. Joo, Opt. Express **28**, 3401 (2020).
19. H. Gu, X. Chen, C. Zhang, H. Jiang, and S. Liu, J. Opt. **20**, 015401 (2017).
20. M. Raissi, A. Yazdani, and G. E. Karniadakis, Science **367**, 1026 (2020).
21. I. Shavrin, L. Lipiäinen, K. Kokkonen, S. Novotny, M. Kaivola, and H. Ludvigsen, Opt. Express **21**, 16901 (2013).